Submitted to *Journal of the Atmospheric Sciences*, April 2004

Diagnostic Comparison of Meteorological Analyses during the 2002 Antarctic Winter

Gloria L. Manney,[1,2] Douglas R. Allen,[3] Kirstin Krüger,[4] Barbara Naujokat,[4] Michelle L. Santee,[1] Joseph L. Sabutis,[5] Steven Pawson,[6,7] Richard Swinbank,[8] Cora E. Randall,[9] Adrian J. Simmons,[10] and Craig Long[11]

Abstract. Several meteorological datasets, including UK Met Office (MetO), ECMWF (European Centre for Medium-Range Weather Forecasts), NCEP (National Centers for Environmental Prediction), and NASA's GEOS-4 (Goddard Earth Observation System) analyses, are being used in studies of the 2002 southern hemisphere (SH) winter, which included the first major warming ever observed in the SH. We compare diagnostics to assess how these studies may be affected by the meteorological data used. Temperature structure and evolution usually agree well between the analyses. Exceptions are the NCEP/NCAR Reanalysis (REAN) and NCEP/DOE Reanalysis-2 (REAN2) datasets, in which severe lower-stratospheric temperature biases result in lower estimates of polar processing potential. SH polar temperatures in ECMWF's ERA-40 reanalysis show unrealistic oscillatory structure in the vertical, so both long-term reanalyses are unsuited for detailed studies relying on stratospheric temperatures in the SH 2002 winter. Temperature history diagnostics related to polar processing show fair agreement between MetO, operational ECMWF, NCEP/CPC (Climate Prediction Center) and GEOS-4 analyses. Winds and wave diagnostics give a consistent picture of the large-scale dynamics of the SH 2002 winter from each dataset, arguing for high confidence in observational studies based on these quantities. However, REAN/REAN2 fields show increasing differences from other analyses between $\sim$30 and 10 hPa (their top level), and quantitative agreement between all analyses worsens in the upper stratosphere. The analyses show substantial differences in the evolution of the upper-stratospheric vortex, with an inferior representation in NCEP/CPC objective analyses. Polar vortex transport barriers are similar in all analyses, but there is little consensus on the amount or patterns of mixing. REAN/REAN2 analyses are not recommended for detailed studies, especially those related to polar processing; the operational assimilated datasets (ECMWF, MetO and GEOS-4) are preferred over the NCEP/CPC objective analyses for most applications. The differences shown here imply that it is most important to assess the choice of analyses for detailed transport studies (including polar process modeling) and studies involving synoptic evolution in the upper stratosphere.

[1]Jet Propulsion Laboratory, California Institute of Technology, Pasadena, California, USA.

[2]Department of Natural Sciences, New Mexico Highlands University, Las Vegas, New Mexico, USA.

[3]Remote Sensing Division, Naval Research Laboratory, Washington, DC, USA.

[4]Institut für Meteorologie, Freie Universität Berlin, Germany.

[5]School of Education and Department of Mathematical Sciences, New

1. Introduction

The first major stratospheric sudden warming ever observed in the southern hemisphere (SH) occurred in late September 2002 (e.g., *J. Atmos. Sci.*, Special Issue, Vol. ##, No. ##, hereinafter *JAS*), and the stratospheric circulation that winter was much more dynamically disturbed than is typical in the SH (e.g., Allen et al., 2003; Krüger et al., 2004; Newman and Nash, 2004; Scaife et al., 2004). The unusually warm and disturbed winter, and the September major warming, led to the disappearance of polar stratospheric clouds (PSCs) and cessation of Antarctic ozone loss earlier in the season than usual (e.g., Hoppel et al., 2003; Nedoluha et al., 2003; Sinnhuber et al., 2003; Feng et al., 2004).

Examination of the unique 2002 SH winter includes observational and modeling studies of transport, ozone chemistry, the dynamics of and mechanisms leading to the major warming, and the unusual dynamical situation throughout the winter. Nearly all of these studies use meteorological analyses (wind, geopotential height and temperature data) from one or more operational assimilation systems. Manney et al. (2003) showed that, for the northern hemisphere (NH) winter lower stratosphere, significant differences in the results of polar processing studies were expected depending on the dataset used.

Here, we compare the most commonly used meteorological datasets during the 2002 SH winter. Diagnostics are representative of calculations that might be done in several types of studies, including those of large scale dynamics and wave propagation, synoptic evolution, transport barriers, mixing and filamentation, and polar processing. By choosing diagnostics related to those used in scientific studies, we hope to elucidate uncertainties that may arise from the choice of meteorological data used.

2. Data and Analysis

The meteorological datasets used are from the UK Met Office (MetO), the US National Centers for Environmental Prediction (NCEP)/Climate Predication Center (CPC) (NCEP/CPC data), the European Centre for Medium-Range Weather Forecasts (ECMWF), NASA's Global Modeling and Assimilation Office (GMAO), and the NCEP/National Center for Atmospheric Research (NCAR) Reanalysis (REAN). In addition, the NCEP/Department of Energy (DOE) "Reanalysis-2" data (REAN2) and ECMWF's ERA-40 reanalysis data are examined. Several of the meteorological datasets used here are described in some detail by Manney et al. (2003) and by Randel et al. (2004), but there have been some changes since then. The NCEP/CPC data are the same as described in those papers, except that the data from GDAS, NCEP's operational assimilation system, have been used at all levels through 10 hPa since May 2000 (as opposed to 100 hPa earlier). The REAN data are produced by the same systems as described by Manney et al. (2003), but a problem mentioned there with TOVS (Tiros Operational Vertical Sounding) filtering has been corrected. The Met Office upgraded to a three-dimensional variational (3D-Var) system that assimilates satellite radiances rather than retrieved temperatures in November 2000 (e.g., Lorenc et al., 2000; Swinbank et al., 2002). The ECMWF operational analyses use a 4D-Var system; changes in analyses since 2000 include an increase in model resolution from T319 to T511; the operational ECMWF analyses for the 2002 SH winter, as well as special reruns for the period of the SH major warming, are described by Simmons et al. (2004). Some of the diagnostics have also been calculated using ECMWF data from these reruns (ECMWF-R data), which were done with an updated (operational in January 2003) assimilation system and a correction for a weak computational instability in the forecast model.

Rather than the GEOS (Goddard Earth Observation System)-3 data from GMAO used by Manney et al. (2003), we use here the new GEOS-4.0.2 (referred to hereinafter as GEOS-4) data, which have been operational since October 2002. The GEOS-4 assimilation system uses the same Physical Space Statistical Analysis Scheme (Cohn et al., 1998) as in GEOS-3, but with a new dynamical core (Lin, 2004); further details are given by Li et al. (2004). Re-evaluation of the diagnostics shown by Manney et al. (2003) indicates that GEOS-4 behavior is much more similar to other analyses than was that in GEOS-3; other diagnostics also show improvements over GEOS-3 (S. Pawson et al., "Stratospheric meteorology and transport analyzed in NASA's GEOS-4 data assimilation system", in preparation).

In addition to the REAN data, a similar, but improved, dataset is available in the NCEP/DOE "Reanalysis-2" (REAN2) (Kanamitsu et al., 2002). REAN2 uses the same underlying model and assimilation system as REAN, but with a number of corrections. Thus, it still has many of the same limitations (low-resolution, older forecast model, assimilation of retrieved temperatures rather than radiances, 3D-Var rather than 4D-Var assimilation, poor vertical resolution in the stratosphere, top analysis level at 10 hPa), but is considered to be an overall improvement. Kanamitsu et al.

Mexico Highlands University, Las Vegas, New Mexico, USA.
[6]NASA/Goddard Space Flight Center, Greenbelt, MD.
[7]Goddard Earth Science and Technology Center, UMBC, Baltimore, MD
[8]Met Office, Exeter, UK.
[9]Laboratory for Atmospheric and Space Physics, University of Colorado, Boulder, CO, USA.
[10]European Centre for Medium-Range Weather Forecasts, Reading, UK.
[11]NOAA Climate Prediction Center, Camp Springs, MD.

(2002) note that the changes have made some differences in the stratosphere, in particular in SH temperatures and in equatorial divergent winds. As will be shown below, results for REAN and REAN2 data are much more similar to each other than either one is to the other analyses. Except where otherwise noted, we show REAN2 data here.

ECMWF's ERA-40 Reanalysis data were produced through August 2002. While these do not cover the period of the major warming, they have been used for a number of analyses in the SH stratosphere, including assessing whether events comparable to the 2002 major warming may have occurred previously in the SH (e.g., Simmons et al., 2004). Some comparisons of ERA-40 with the other datasets are therefore included. Simmons et al. (2004) briefly describe the 3D-Var assimilation system used for ERA-40, and some artifacts seen in Antarctic stratospheric temperatures in those analyses; early results for zonal mean winds and temperatures from ERA-40 are compared with other analyses by Randel et al. (2004). In August 2002, but not in the previous months of that winter, AMSU (Advanced Microwave Sounding Unit) data from NOAA-16 were used in the assimilation; as will be seen below, this had a detrimental effect on the ERA-40 temperature analyses in August 2002.

The NCEP/CPC data are provided on a 65×65 polar stereographic grid for 12 UT. Here, these are interpolated to a $2.5^\circ\times5^\circ$ latitude/longitude grid, and balanced winds are calculated from the geopotential height (Randel, 1987; Newman et al., 1989). The REAN and REAN2 data are archived on a $2.5\times2.5^\circ$ grid, and the daily average data are used; Manney et al. (2003) found insignificant differences using daily average versus 12 UT data. MetO data are available on a $2.5\times3.75^\circ$ grid at 12 UT. The ECMWF operational and ERA-40 data used are for 12 UT and have been interpolated to $2.5\times2.5^\circ$. ECMWF-R data are provided at $1.25\times1.25^\circ$, and 12 UT data are used here. GEOS-4 data are available four times daily on a $1\times1.25^\circ$ grid, but only 12 UT data are used for most of the comparisons shown here. 12 UT GEOS-4 data interpolated to a $2\times2.5^\circ$ grid are also used to examine some effects of resolution.

Potential vorticity (PV) is calculated from each dataset using the same algorithm (Newman et al., 1989; Manney et al., 1996), adapted to run at higher resolution for the GEOS-4 and ECMWF-R data. Several diagnostics shown are based on trajectory calculations, which are done isentropically using the trajectory code described by Manney et al. (1994b). Eliassen-Palm (EP) fluxes and other wave propagation diagnostics are calculated as described by Sabutis (1997); the datasets were interpolated to a common grid prior to the EP flux calculations. Each analysis is provided on different pressure levels, though many levels (e.g., 100, 50, 30, 10 hPa) are common to most datasets. When a common vertical grid is needed, the datasets are interpolated linearly in log(p) to the Upper Atmosphere Research Satellite (UARS) pressure levels on which the MetO data are provided, comprising six levels per decade in pressure, equally spaced in log(p). Radiosonde data compared to the analyses here were made available by the Global Telecommunication System of the World Meteorological Organization (WMO), as described by Krüger et al. (2004).

3. Overview of Temperature Structure

Randel et al. (2004) compare middle atmosphere zonal mean temperatures and winds from several analyses, focusing on climatological aspects such as monthly means and interannual variability. In contrast, we are primarily interested in comparisons of day-to-day evolution during one particular winter. An overview of the temperature structure and evolution gives us a first-order picture of fundamental areas of agreement or disagreement between the analyses.

Radiosonde temperatures are commonly used for comparison in validation studies and forecast verification. Simmons et al. (2004) showed good agreement between temperature changes related to vortex evolution in ECMWF analyses and forecasts and radiosonde observations. Though radiosonde observations are used as inputs in each of the analyses shown here, none of the assimilation systems weight the SH radiosondes during this periods highly; thus, these comparisons provide significant information on how well the analyses capture the detailed local temperature evolution observed by radiosondes. Figure 1 shows temperatures at 20 and 50 hPa from observations at three representative radiosonde stations in the Antarctic during August through October 2002, along with temperatures from the meteorological analyses interpolated (bilinearly in latitude and longitude and linearly in log(p) in the vertical, with no time interpolation) to those locations. (REAN, reduced-resolution GEOS-4, and ECMWF-R datasets, not shown, give nearly identical results to REAN2, GEOS-4 and ECMWF, respectively.) The major warming can be readily identified in the Amundsen-Scott and Neumayer temperatures as a sudden, prolonged increase beginning around 20 September (day 40); an earlier strong minor warming is apparent at Neumayer around 1 September (day 31), and minor warmings in August are seen at Syowa. For the most part, all of the analyses follow the radiosondes closely. The REAN2 data, however, are often warmer than radiosondes and other analyses at 20 hPa at low temperatures (e.g., Amundsen-Scott and Neumayer in August and early September). NCEP/CPC analyses also show higher values at 20 hPa in August, when temperatures are very low. In addition, REAN2 data commonly cut off below the highest values observed by ra-

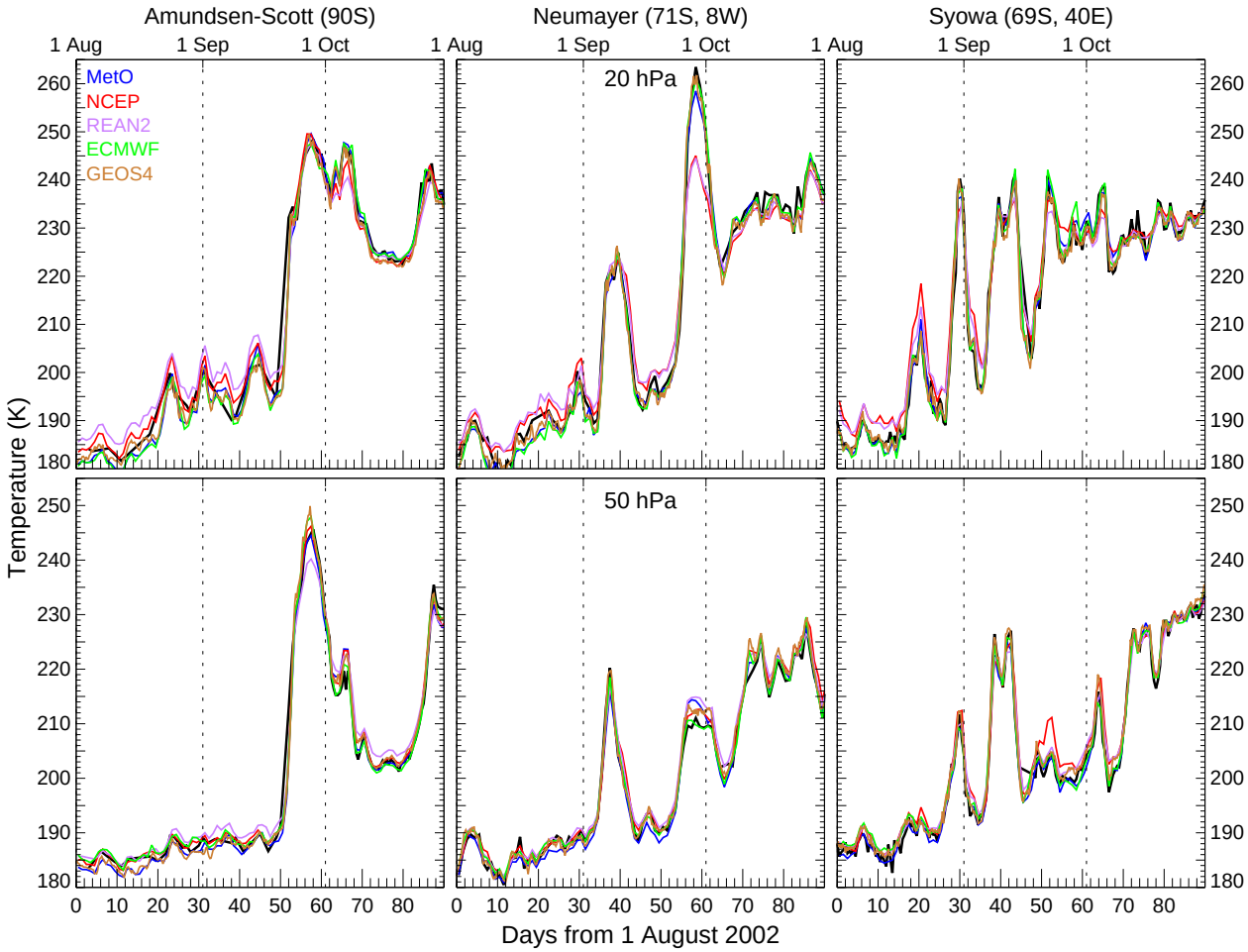

Figure 1. Time Series from 1 August through 31 October 2002 of radiosonde observations (thick black lines) at 20 and 50 hPa, compared with analyses interpolated to radiosonde locations. Locations of Amundsen-Scott, Neumayer, and Syowa are 90°S; 71°S, 352°E; and 69°S, 40°E; respectively.

diosondes (e.g., Amundsen-Scott at 50 hPa and Neumayer at 20 hPa around 28 September (day 58)) and obtained from other analyses. This failing is also, though less frequently, seen in the NCEP/CPC data (e.g., Neumayer at 20 hPa near 28 September). Differences between the REAN datasets and the others that may account for this behavior include the lower model resolution and fewer levels in the stratosphere, and the assimilation of retrieved temperatures rather than radiances. While the data below 10 hPa in the NCEP/CPC analyses come from a higher resolution model, the interpolation to the 65×65 polar stereographic grid (which substantially degrades the resolution at these high latitudes) may result in lower interpolated peak temperatures. At 10 hPa (not shown), similar differences are seen, but here there are also several occasions when the MetO analyses overshoot the maximum temperatures seen in the radiosonde data, including during several minor warmings in August and early September.

Similar differences between analyses are apparent for fixed points removed from radiosonde stations (not shown), with the REAN2 and NCEP/CPC analyses tending to cut off the extreme values, and MetO analyses showing higher maxima at 10 hPa. Figure 2 shows minimum and maximum temperatures poleward of 40°S at 50, 30 and 10 hPa during the SH 2002 winter. While in the earlier months, the maxima are often near the equatorward edge of the domain (40°S), after early August the are always at high latitudes (poleward of ∼55°S). Maximum temperatures typically agree closely at 50 and 30 hPa until mid-August, when dynamical activity (seen as larger temperature fluctuations) increases; the exceptions are GEOS-4 and ERA-40 temperatures at 50 hPa, which are consistently 1-2 K higher than those in the other analyses during May through July. A larger spread among the analyses is seen at 10 hPa, commonly as much as ∼10 K, with REAN2 and NCEP/CPC analyses showing lower temperatures and substantially underestimating maxima, and the MetO data typically showing highest temperatures. As dynamical activity increases, REAN2, and to a lesser degree NCEP/CPC, tends to underestimate the maxima seen in other analyses even at the lower levels. During the major warming, the peak temperatures vary by over 30 K, and temperatures in ECMWF, MetO and GEOS-4 are the highest in the Antarctic record since ∼1950.

Minimum temperatures show good consistency in overall evolution and day-to-day variations, but quantitative similarity is seen only at 50 hPa, where the spread among the analyses is typically ∼2-3 K. At 30 hPa, REAN2 and ERA-40 temperatures are biased high with respect to the others by ∼3-6 K. MetO and ERA-40 temperatures are biased low by ∼1-2 K at 50 hPa. The shift from low to high bias in ERA-40 temperatures shows the vertically oscillatory Antarctic temperature structure reported by Randel et al. (2004) and Simmons et al. (2004). Also, as noted above, differing inputs into ERA-40 in August 2002 had a detrimental effect on the analyses, resulting in further degradation of the temperature structure (e.g., very low minimum ERA-40 temperatures at 10 hPa).

Figure 3 shows time/pressure cross-sections of 60°S zonal mean temperature from MetO, NCEP/CPC, ECMWF, GEOS-4, REAN-2 and ERA-40 datasets. The unrealistic ERA-40 temperature structure in August is readily apparent, and higher minimum temperatures near 50-15 hPa result from the vertical oscillations in temperature. Thus, the ERA-40 temperatures are not recommended for detailed analyses of temperature evolution in the 2002 SH winter. The REAN2 analyses show higher minima and lower maxima than the other analyses, arguing for caution in using this dataset for detailed studies of SH temperature evolution. In the remaining four datasets, day-to-day temperature evolution agrees quite well up to ∼5 hPa, with typical differences on the order of 3 K or less. The development of and recovery from the major warming in particular shows quantitative agreement. Differences are seen near 1-3 hPa, where GEOS-4 temperatures level off at lower values, while ECMWF, NCEP/CPC and MetO temperatures continue to increase more rapidly. Larger differences in the upper stratosphere are expected, since TOVS satellite soundings (used in all the analyses) stop at 1-2 hPa, and provide only about three pieces of information for a layer over 20 km thick (e.g., Li et al., 2004). Li et al. (2004) show that the GCM formulation, in particular the gravity wave drag parameterization, leads to large analyzed temperature (and wind) differences near the stratopause, including differences in the level of the stratopause.

These broad comparisons show overall agreement between MetO, NCEP/CPC, ECMWF and GEOS-4 temperature structure and evolution (though NCEP/CPC fields occasionally underestimate extrema), and indicate that ERA-40 and REAN2 temperatures should be used, at best, with great caution for detailed studies in the 2002 SH winter. In the following sections, we turn to more detailed comparisons of fields and diagnostics used in scientific studies.

4. Large-Scale Dynamics

Many studies focus on the large-scale dynamics of the SH 2002 winter (e.g., *JAS*). Several observational studies examine large-scale dynamics throughout the winter (e.g., Krüger et al., 2004; Newman and Nash, 2004; Hio and Yoden, 2004; Scaife et al., 2004), including winds, temperatures and wave diagnostics. Some also focus on synoptic evolution during the major warming (e.g., Krüger et al., 2004; Manney et al.,

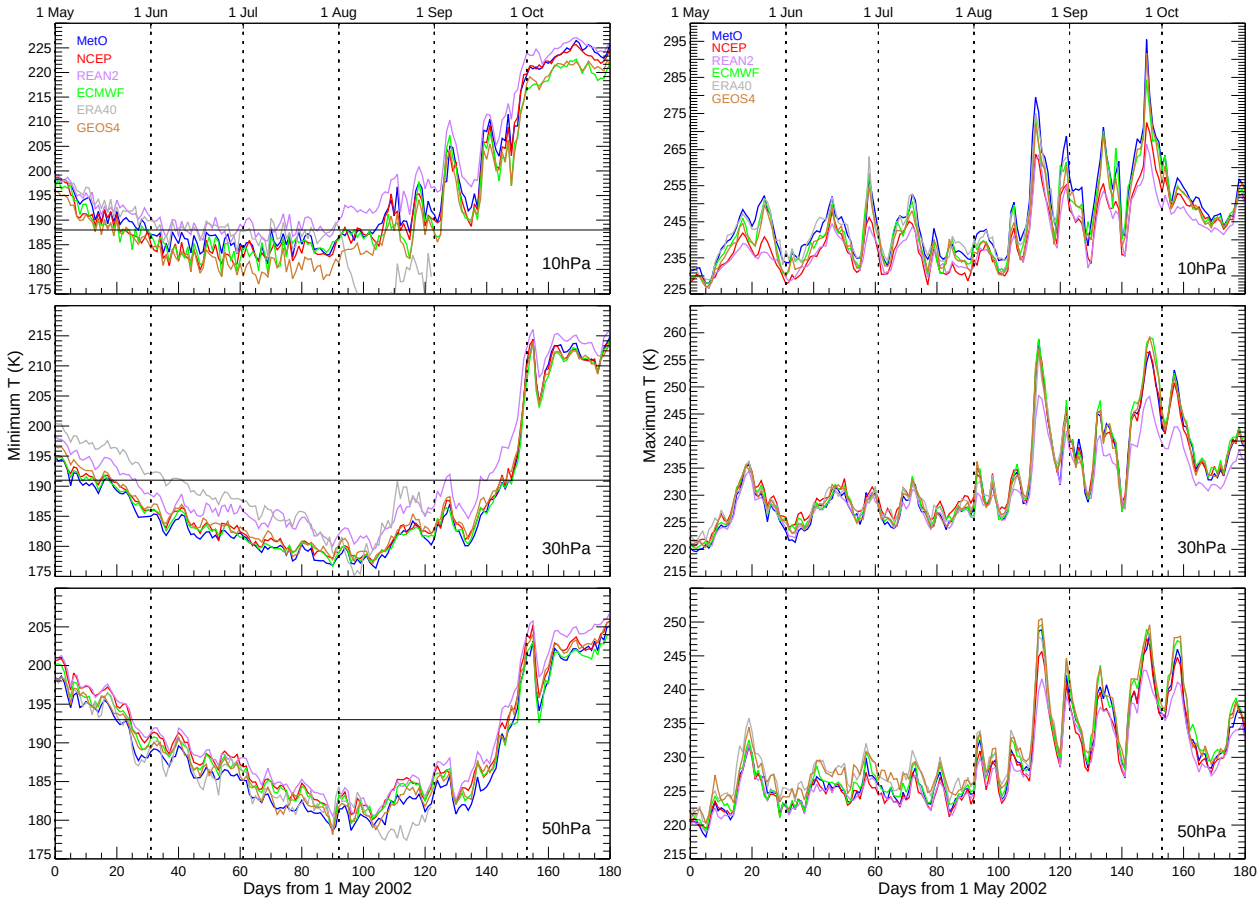

Figure 2. Minimum (left) and Maximum (right) temperatures at 10, 30 and 50 hPa (top to bottom) poleward of 40°S during the 2002 Antarctic winter, from MetO (blue), NCEP/CPC (red), REAN2 (lavender, REAN values are very similar), ECMWF (green, ECMWF-R values are very similar), ERA-40 (grey) and GEOS-4 (brown) analyses.

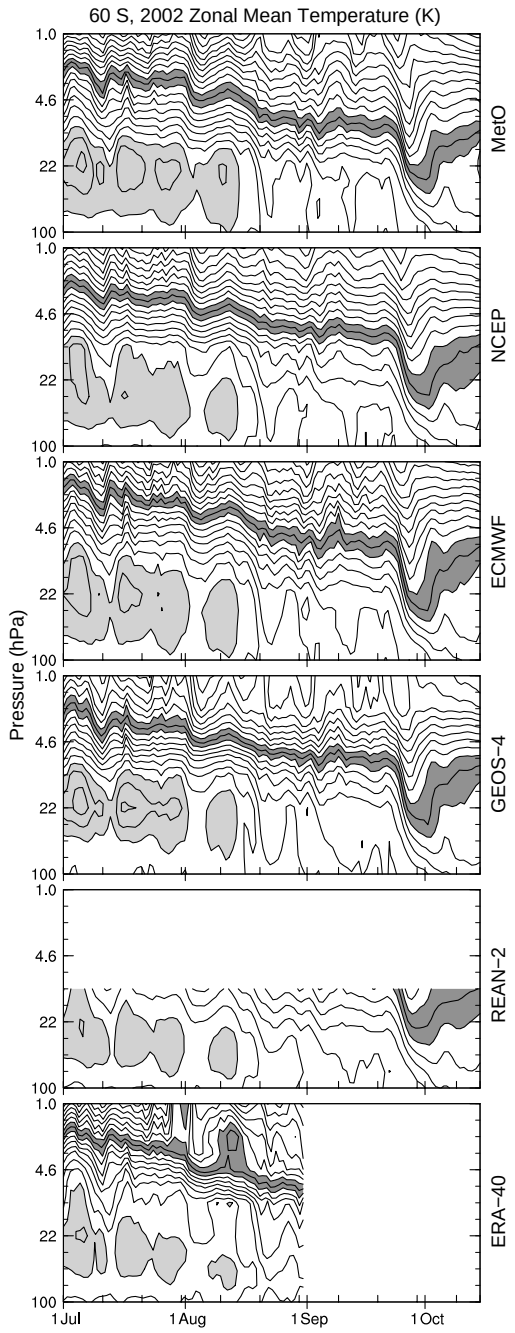

Figure 3. Zonal mean temperature (K) at 60°S as a function of pressure and time from six meteorological analyses (MetO, NCEP/CPC, ECMWF, GEOS-4, REAN2 and ERA-40) for July through October 2002 (ERA-40 only through August). Contour interval is 3 K, with light shading from 195 to 207 K, and dark shading from 228 to 234 K.

2004; Simmons et al., 2004), including the day-to-day evolution of winds, PV and other fields; Manney et al. (2004) use several analyses to drive mechanistic model simulations of the major warming. Gray et al. (2004) and Harnik et al. (2004) focus on the possible effects of tropical and subtropical winds on polar dynamics and the development of the major warming. In this section, we compare winds and diagnostics used in studies of large-scale dynamics.

a. Winds and Wave Propagation During the SH 2002 Winter

All analyses show excellent agreement in high-latitude zonal mean winds (Figure 4) at and below 10 hPa. Each shows the 10 hPa wind reversal on 25 September and return to westerlies on 30 September during the major warming, and agrees on the timing and intensity of earlier minor warmings. As shown by Manney et al. (2004), MetO, NCEP/CPC, ECMWF and GEOS-4 10-hPa high-latitude winds typically agree within 1–2 m/s during September–October; however, REAN2 gives weaker westerlies prior to, and weaker easterlies during, the major warming (by up to ∼6–10 m/s) near 10 hPa. Winds in the ERA-40 analyses are consistent with those in other analyses despite the unrealistic temperature structure (section 3) because the temperature anomaly is oscillatory (so the wind shear related to it integrates to near zero in the vertical) and of broad horizontal scale (so the meridional temperature derivative related to it is small). Even in the upper stratosphere there is good qualitative agreement in wind variations. The most noticeable difference is the variation between analyses in the level of maximum winds during periods when westerlies strengthen, with GEOS-4 and ERA-40 showing maxima at or above 1 hPa, and the other analyses showing maxima near 2–3 hPa. There is also a difference of up to four days (between NCEP/CPC, earliest, and MetO, latest) in the date of the return to westerlies after the major warming in the upper stratosphere. As discussed further in sections 3 and 4(*b*), increasing differences are expected in the upper stratosphere, where the analyses are more dependent on the underlying GCMs (e.g., Li:etal:2004).

Figure 5 shows 10°S winds from April through October, to highlight the evolution of the semi-annual oscillation (SAO) and quasi-biennial oscillation (QBO) in the SH tropics (NCEP/CPC winds are not shown, since the balanced wind calculations result in gross underestimation of tropical wind fluctuations, e.g., Randel et al., 2004, and REAN/REAN2 analyses are not shown since they don't extend into the upper stratosphere). Low-latitude easterlies influence wave propagation through the polar stratosphere, and were anomalously strong in the middle to upper stratosphere during the 2002 SH winter (Gray et al., 2004; Harnik

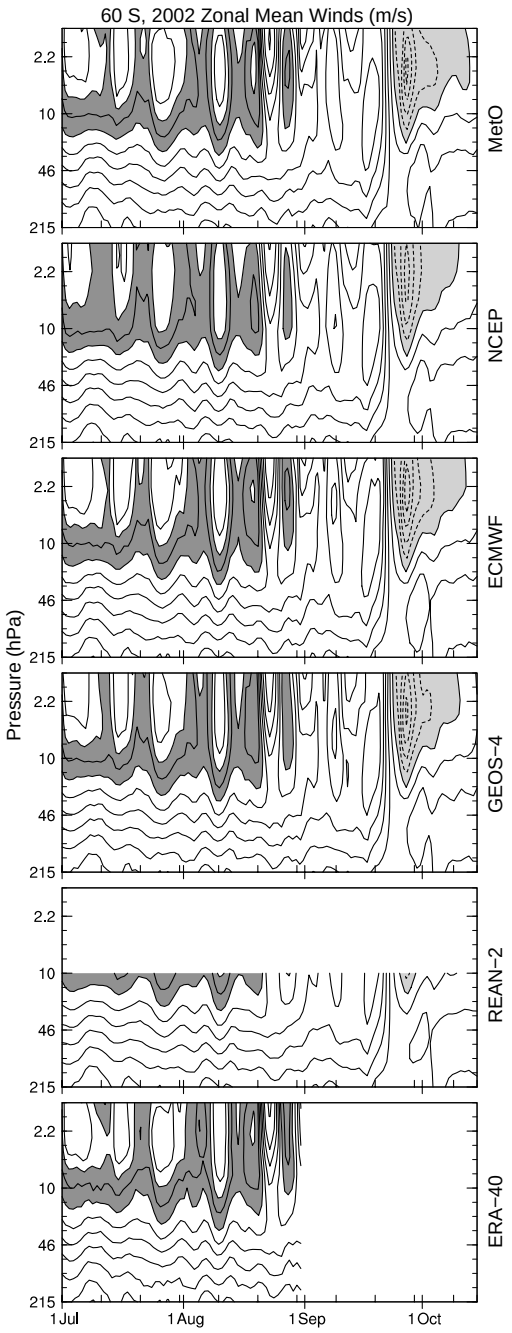

Figure 4. Zonal mean winds (m/s) at 60°S as a function of pressure and time from six meteorological analyses (MetO, NCEP/CPC, ECMWF, GEOS-4, REAN2 and ERA-40) for July through October 2002 (ERA-40 only through August). Contour interval is 10 m/s, with light shading for values less than zero and dark shading from 70 to 90 m/s.

et al., 2004). MetO, ECMWF, GEOS-4 and ERA-40 analyses show very similar regions of QBO westerlies in the lower stratosphere; those in the REAN2 analyses (not shown) are up to ∼4 m/s weaker. There are differences of up to 8 m/s in the strength of the maximum easterlies in the upper stratosphere. Gray et al. (2004) noted significant differences in the SAO between MetO and ERA-40 equatorial winds, with MetO winds showing westerlies only above 1 hPa; this difference is apparent in the 10°S winds shown here, with MetO fields showing no westerlies (top of plot is 1 hPa) and the operational ECMWF, GEOS-4 and ERA-40 fields all showing westerlies over similar regions. Even between these, though, there are significant differences in the magnitude and time evolution of upper stratospheric westerlies. As noted in section 3, the only data constraint in the upper stratosphere is TOVS, which gives information on the thermal structure in broad layers. When combined with the weak balance assumption at low-latitudes, the GCMs are the dominant factor in determining these wind fields.

Diagnostics of wave propagation calculated from meteorological analyses are important to many dynamical studies (e.g., Krüger et al., 2004; Harnik et al., 2004; Newman and Nash, 2004; Scaife et al., 2004). Figure 6 shows the EP flux divergence at 22 hPa at 68°S (the latitude where largest fluxes are observed) and the vertical EP flux component at 100 hPa and 60°S (latitude of largest values) during August through October. The vertical component at 100 hPa, representing the upward propagation in the lower stratosphere, is very similar in all the analyses, with differences of only ∼15% (between MetO and REAN (lowest) and GEOS-4 (highest)) in maximum amplitude of the large upward wave pulse that triggered the major warming. However, as shown by Manney et al. (2004), quite small differences in the vertical EP flux component may result in large differences in propagation through the stratosphere. EP flux divergences also show generally good agreement at all levels, but at 22 hPa (the highest level where calculations from REAN are reliable) the magnitudes are notably smaller in the REAN calculations. Harnik et al. (2004) also showed generally good agreement between wave propagation diagnostics from NCEP/CPC and REAN data.

Overall, winds and wave propagation diagnostics throughout the winter give a consistent picture from all the analyses. Agreement is close enough that the choice of dataset for observational studies should not significantly affect their results. The only caution would be in using REAN/REAN2 winds or EP fluxes for detailed studies at the top few levels (between about 30 and 10 hPa) they are available.

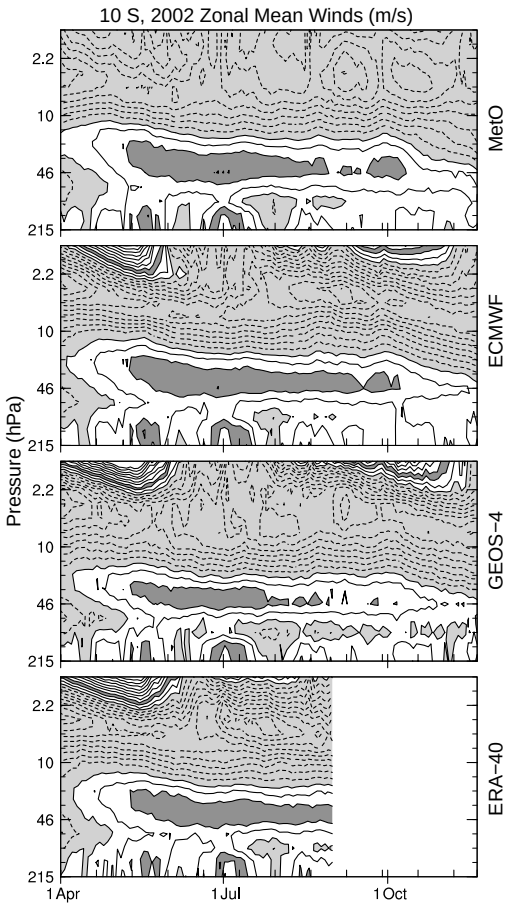

Figure 5. Zonal mean winds at 10°S as a function of pressure (from 215 to 1 hPa) and time from MetO, ECMWF, GEOS-4, and ERA-40 meteorological analyses for April through October 2002 (ERA-40 only through August). Contour interval is 4 m/s; light shading shows values less than zero, and dark shading values from 8 to 12 m/s.

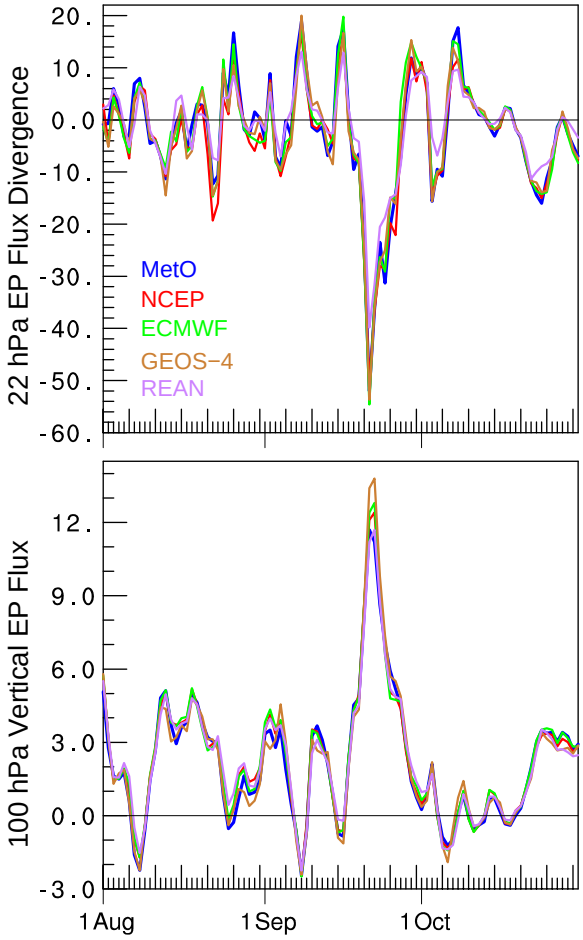

Figure 6. (top) EP flux divergence (expressed as wave-driving, m/s/d) at 68°S from five meteorological analyses at 22 hPa and (bottom) vertical EP flux component (10^{12} m/s^2) at 100 hPa and 60°S, for August through October 2002 in the SH.

b. Synoptic Structure and Evolution During the Major Warming

As shown by Manney et al. (2004), and as is typical during NH major warmings (e.g., Fairlie et al., 1990; Manney et al., 1994a), temperature gradients are strongly enhanced along the vortex edges prior to and during the peak of the warming, forming tilted baroclinic zones reminiscent of upper tropospheric fronts. Figure 7 shows cross-sections of temperature around 60°S for the analyses that extend into the upper stratosphere. Each shows very similar temperature gradients along the baroclinic zones in the lower stratosphere, up to ∼10 hPa (the REAN2 analyses, not shown, have weaker temperature gradients in the lower stratosphere). In contrast, there are substantial differences in the upper stratosphere. For those analyses with data routinely available above 1 hPa (MetO, NCEP/CPC, and GEOS-4), there are significant differences in both the location and the temperature of the stratopause. In particular, the level of maximum temperatures in the western hemisphere and the structure of the local temperature maximum near 2 hPa and 0° longitude vary substantially. At stratopause level there are fewer data being assimilated and the satellite temperature observations have very poor vertical resolution; as shown by Li et al. (2004), the analyzed temperatures in the upper stratosphere are thus highly sensitive to the underlying GCM formulation. As there are very few data available for comparison at these levels, it is difficult to suggest which analyses may be most accurate, although the sharpness of the stratopause structure in the MetO analyses (e.g., the protrusion of temperatures greater than ∼260 K east of 100°E at ∼0.5 hPa) seems unlikely to be realistic. The mechanistic model simulation described by Manney et al. (2004) shows a stratopause morphology similar to the smoother transitions in NCEP/CPC and GEOS-4 despite being initialized with MetO data.

Enhanced vertical velocities along the baroclinic zones are instrumental in determining the anomalous transport during stratospheric warmings (e.g., Manney et al., 1994a, 2004). Figure 8 shows cross-sections of ω, the vertical velocity in pressure coordinates, from MetO, ECMWF, and GEOS-4, and from the UGAMP (UK Universities Global Atmospheric Modelling Project) Stratosphere-Mesosphere Model (USMM) simulation described by Manney et al. (2004). Detailed comparison is not feasible, since the different centers provide different averages: MetO ωs are six-hour averages valid at 12 UT; ECMWF ωs are snapshots at 12 UT (hence noisier fields); 12 UT values for GEOS-4 ωs are obtained by averaging the six-hour average values valid at 9 and 15 UT; USMM values are synoptic at 12 UT. Nevertheless, it is instructive to get an impression of how the analyses represent the enhanced vertical velocities along the baro-

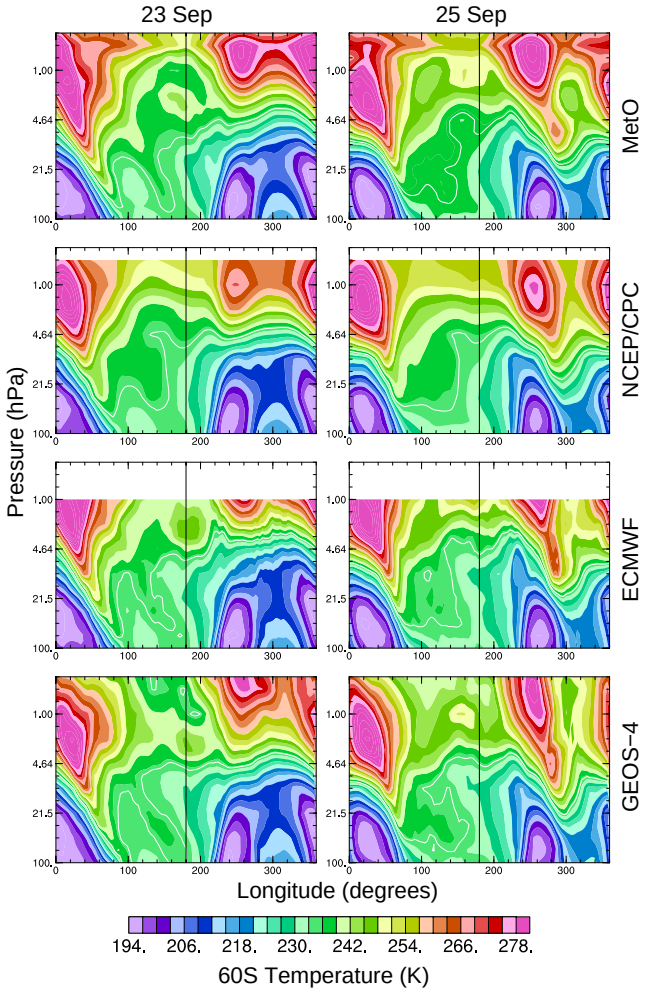

Figure 7. Cross-sections of temperature around 60°S on 23 and 25 September 2002 from each of four meteorological analyses. The 235 K contour is outlined in white.

clinic zones during the warming. To obtain more comparable fields, we have averaged over three days, 24-26 September, during the peak of the warming when the vortex is most strongly tilted and vertical velocities are strongest (e.g., Manney et al., 2004). All of the analyses appear to capture very similar magnitudes and patterns of strongly enhanced downward motion near 40°-140°E, with maximum values typically a bit larger than those in the USMM simulation; region of enhanced downward motion along the other vortex edge, ∼260°-320°E, is also very similar. Regions of enhanced upward motion are qualitatively similar in all analyses (except for the suggestion of a significant region of upward motion near 180°E in ECMWF analyses), but variations in magnitude are larger, with the model showing significantly weaker upward motion near 0° and 220°E than the analyses. Thus, although the vertical velocities from assimilation systems are generally known to be problematic for use in large-scale transport calculations (e.g., Schoeberl et al., 2003, and references therein), all the analyses capture the large scale patterns of enhanced vertical velocities associated with the major warming, and the magnitudes of the vertical velocities are in reasonable agreement with each other and with the USMM simulation. The good quality of the forecasts produced by ECMWF (Simmons et al., 2004) suggests that their synoptic vertical velocities must be realistic, and hence overall agreement with the other datasets indicates reasonable quality in all the synoptic vertical velocities during the major warming.

Although, as shown in section 4(*a*), the mean features of the large scale stratospheric flow are similarly represented in each of the analyses, there are often small, but potentially significant, differences in the synoptic fields and evolution. These can become particularly important in PV calculations, where differences may be magnified because it is a highly derived field. In the middle and lower stratosphere (not shown), the differences are modest and largely quantitative. Figure 9 shows upper stratospheric "scaled PV" (sPV, in "vorticity units", e.g., Dunkerton and Delisi (1986), Manney et al. (1994b)) from each of the analyses at 1450 K (∼40-42 km) during the warming, with a few temperature contours overlaid. While the temperatures show close agreement between all analyses (with NCEP/CPC having slightly lower (higher) maxima (minima)), much larger differences are seen between PV fields.

On 24 September the vortex is just splitting in the upper stratosphere. The NCEP/CPC and GEOS-4 analyses show more completely split vortices than the MetO and ECMWF fields. There are also significant differences in vortex strength (i.e., PV gradients along the vortex edge), with strongest (weakest) vortices in ECMWF (NCEP/CPC) analyses, and in the degree to which we can identify air being

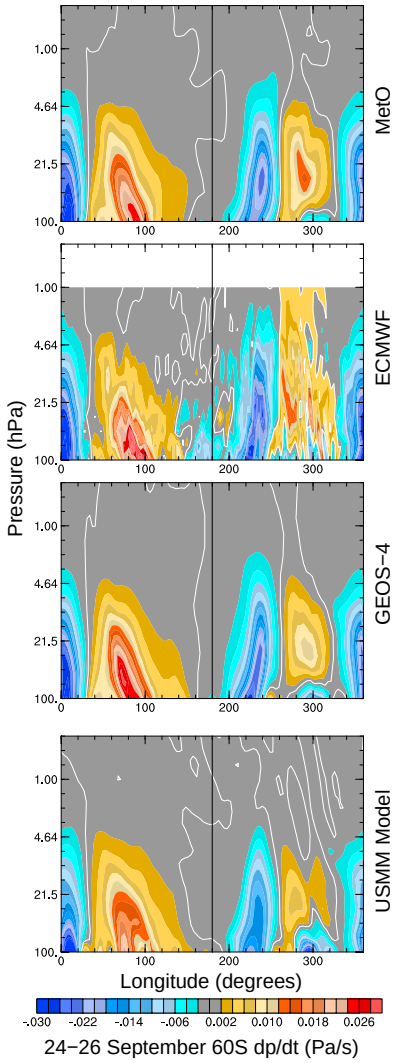

Figure 8. Cross-sections of ω (Pa/s, vertical velocity in pressure coordinates) around 60°S averaged over 24 through 26 September 2002 from MetO, ECMWF, GEOS-4, and REAN2 analyses, and from the USMM simulation of Manney et al. (2004). Values originally provided by each data center represent different time averages, as described in the text. Positive values indicate downward motions; white contour is zero line.

pulled off the larger vortex near 40°S across 180°E. The PV of vortex air entrained into the anticyclone varies as well; air being drawn up from low latitudes and coiling into the anticyclone is suggested in all except the NCEP/CPC analyses, but is best defined in the GEOS-4 fields. On 28 September, the upper stratospheric vortex comprises three widely separated fragments, the largest of them coiled around a strong, confined anticyclone at high latitudes. Not only do the strength and size of the anticyclone vary (with a much weaker anticyclone in the NCEP/CPC analyses), but there are also distinct differences in the shape, strength and position of the vortex fragments. The structure of the interwoven tongues of vortex-edge and low-latitude air is best defined in GEOS-4; however, these features are also seen in ECMWF and are apparent in reduced resolution GEOS-4 fields (not shown), suggesting that we get more information from the high resolution assimilation systems, even when we are studying a reduced-resolution version of those fields.

Compared to the analyses from assimilation systems, PV from the NCEP/CPC objective analyses shows weaker vortices and anticyclones, and fails to capture the filamentary and tongue-like structure suggested in the other analyses. This difference probably results largely from the assimilation-based wind fields used to calculate PV being refined by information from the underlying GCMs beyond what may be derived directly from the increasingly sparse data at these levels; the models' input to defining the vertical temperature gradients involved in the calculation may also play a role, although we suggest that this is less important since temperature cross-sections (Figure 7) indicate structure in the upper stratospheric NCEP/CPC analyses similar to that in other analyses.

Differences in PV such as those shown here can be important in many studies, including defining the level of detail to which we can understand the 3D structure and evolution of the polar vortex. Such differences in detail are also fundamental to understanding the accuracy and reliability of products derived from correlations of trace gases with PV, such as the proxy ozone of Randall et al. (2004), which relies on fitting sparse solar occultation data against PV to reconstruct synoptic fields.

Synoptic evolution during the SH major warming shows a reassuring degree of agreement in most major features. A caveat to this is that the NCEP/CPC objective analysis data give an inferior representation of vortex evolution and structure in the upper stratosphere. The differences in the large-scale dynamical features are such that they may be significant primarily to detailed modeling studies relying on one of these analyses (e.g., Manney et al., 2004), and to detailed studies of the synoptic morphology and evolution of the vortex, especially in the upper stratosphere.

5. Mixing, Transport Barriers and Fine-scale Structure

During the 2002 SH winter, unusually strong wave activity led to greatly enhanced quasi-isentropic transport and mixing, including small-scale mixing with extensive filamentation of material pulled off the vortex (e.g., Allen et al., 2003, many papers in *JAS*). Models and observations of ozone and other trace gases indicated strongly enhanced poleward transport and mixing dominating the trace-gas evolution over the period of the major warming (e.g., Manney et al., 2004; Randall et al., 2004; Siegmund et al., 2004). Konopka et al. (2004) and Marchand et al. (2004) used high-resolution calculations driven with ECMWF winds to quantify transport and mixing of vortex air into midlatitudes. In the following, we examine the representation of these processes in each of the meteorological analyses.

a. Diagnostics of Mixing and Transport Barriers

Figure 10 shows effective diffusivity (K_{eff}, expressed as log-normalized equivalent length) calculated as described by Allen and Nakamura (2001, 2003); an idealized tracer was initialized on 1 April 2002 with the tracer equivalent latitude from Allen and Nakamura (2003), and advected isentropically until November using winds from each of the analyses. K_{eff} provides a measure of mixing and transport barriers (e.g., Haynes and Shuckburgh, 2000a, b; Allen and Nakamura, 2001; Tan et al., 2004), with low values representing transport barriers, and high values representing strong mixing.

The lack of a transport barrier in NCEP/CPC calculations in the equatorial lower stratosphere arises primarily from the use of balanced winds. GEOS-4 and REAN2 also show weaker subtropical barriers than MetO and ECMWF in the lower stratosphere (650 and 520 K). Previous studies (e.g., Rogers et al., 1999; Douglass et al., 2003; Schoeberl et al., 2003; Tan et al., 2004) have shown that assimilated or analyzed datasets give an excess of subtropical transport; thus, the stronger subtropical barriers are expected to be more realistic. The polar vortex transport barrier is similar in all analyses, except in REAN2 at 650 K, where the vortex decays less completely during, and recovers more fully after, the major warming than in the other analyses.

Large differences exist in the regions of enhanced midlatitude mixing at all levels. The MetO and ECMWF calculations typically show most mixing during and after the major warming, while REAN2 shows much less mixing at 520 K than the other analyses during and after the major warming. Overall, maximum midlatitude K_{eff} values at 1450 K are comparable in MetO, ECMWF and GEOS-4, but 15-20% lower in NCEP/CPC; at 850 K, all maximum mixing

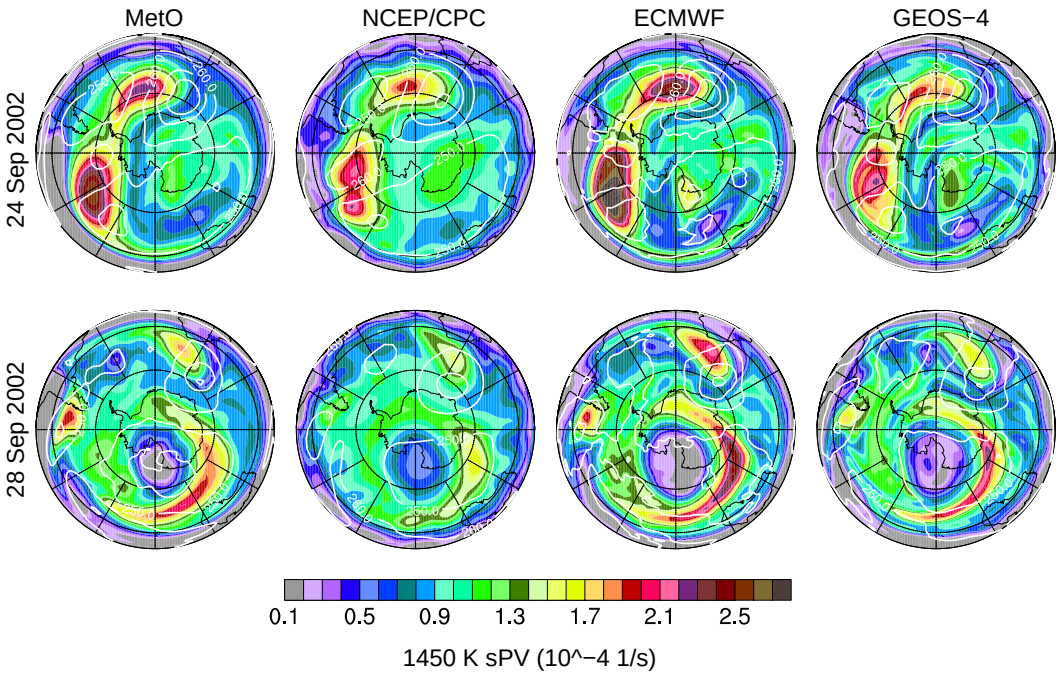

Figure 9. 1450-K sPV maps on 24 and 28 September from each of four meteorological analyses (MetO, NCEP/CPC, ECMWF, and GEOS-4). Temperature contours are overlaid in white; contour interval is 10 K. Domain is from equator to pole with dashed circles at 30° and 60°S; 0° longitude is at the top and 90°E to the right.

values are within 10% of each other, with highest values in GEOS-4. In the lower stratosphere there is more scatter in maximum values, but REAN2 has lowest values (by 10-20%) at both 650 and 520 K. While these differences in the magnitude of the maxima are modest, they are accompanied by differences in timing, location and duration of maximum mixing. Thus, although all the analyses give a comparable representation of the polar vortex, there is no consensus on the amount, patterns and timing of mixing in midlatitudes, nor on the extent of mixing into the polar regions during the major warming. Such variations in mixing between analyses are expected to result in significant differences in transport calculations driven with different analyses.

b. Filamentation

To examine how differences in mixing are manifested in synoptic fields, we show maps of a high-resolution "PV-tracer" at 850 K (Figure 11) during the major warming. Isentropic reverse trajectory (RT) calculations (e.g., Manney et al., 1998, 2000, and references therein) were initialized with sPV. Quite significant differences are seen in the size and strength of the vortex. For instance, a stronger (i.e., larger PV gradients along the edge) and deeper (i.e., higher PV values within) vortex is seen in GEOS-4 analyses, and a smaller and weaker vortex in ECMWF analyses (especially on 25 September). Substantial differences are seen in material pulled off the vortex and entrained into the anticyclone: higher-valued vortex filaments in the anticyclone (90-120°E, 50-70°S on 25 September, 180-270°E, 40-80°S on 3 October) in the GEOS-4 calculations; differences in the position and size of the 3 October filament near 40°S in the 0–90°E sector. Differences in material pulled up from low latitudes include larger tongues of low values in the anticyclone in ECMWF and MetO on 25 September and in GEOS-4 on 3 October, and less low-latitude air pulled up around the vortex regions in all NCEP/CPC calculations compared to those driven with the other analyses (resulting from the use of balanced winds). Differences in local vortex strength (e.g., variations in vortex edge gradients near 330–360°E and between the two vortices on 25 September) could result in different conclusions about the amount of entrainment of material into the vortex. Differences are of similar character at lower levels. REAN2 calculations in the lower stratosphere (not shown) give a weaker and shallower vortex, and show less filamentary structure outside the vortex.

The GEOS-4 calculations show more complex fine-scale structures outside the vortex than the calculations with the other analyses (especially at lower levels). Comparison with the calculations using GEOS-4 data interpolated from

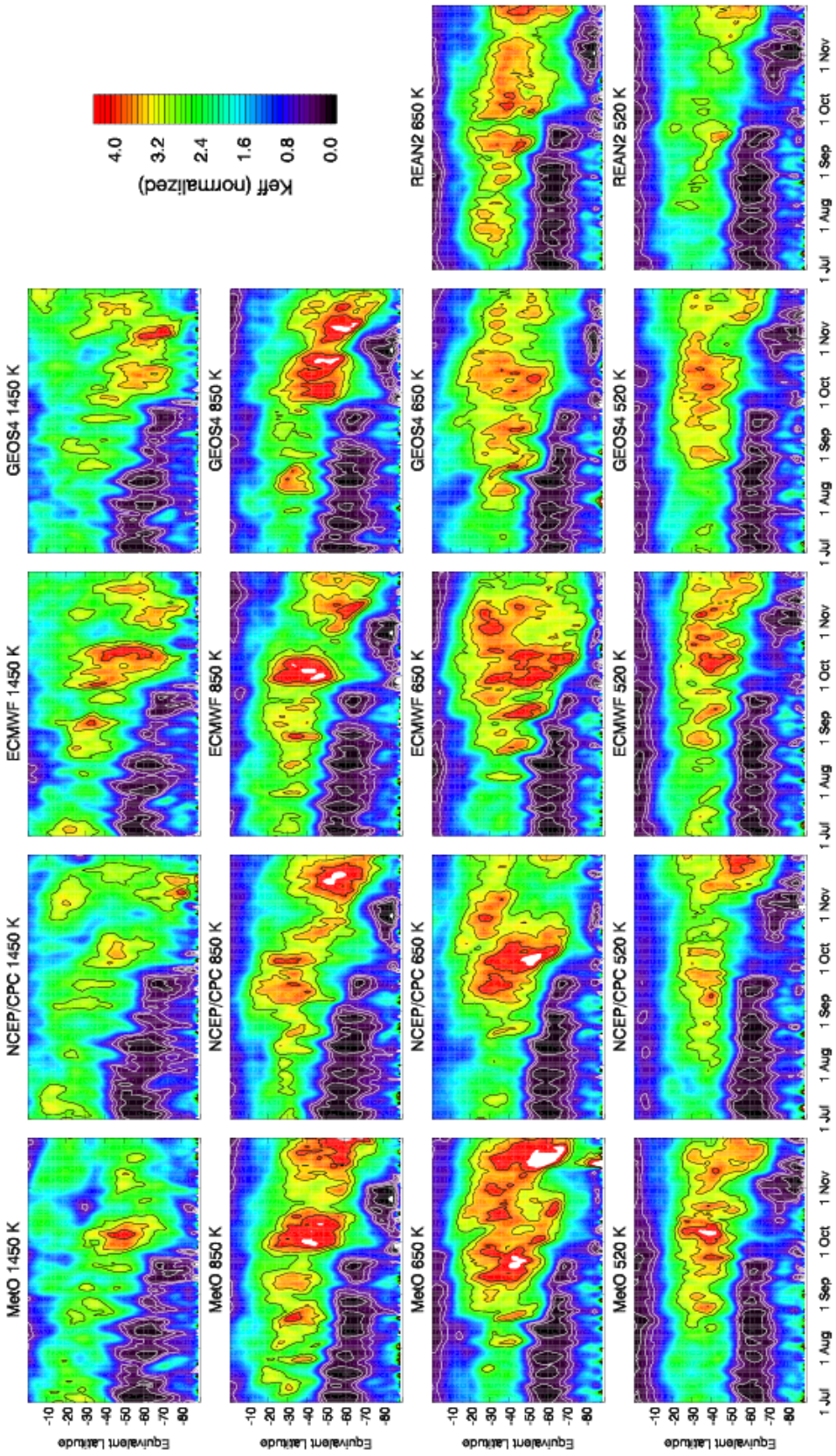

Figure 10. Effective diffusivity, K_{eff}, expressed as log-normalized equivalent length, at 1450, 850, 650 and 500 K in the SH late winter and spring (July through November) 2002, calculated using the model of Allen and Nakamura (2001) from five meteorological datasets.

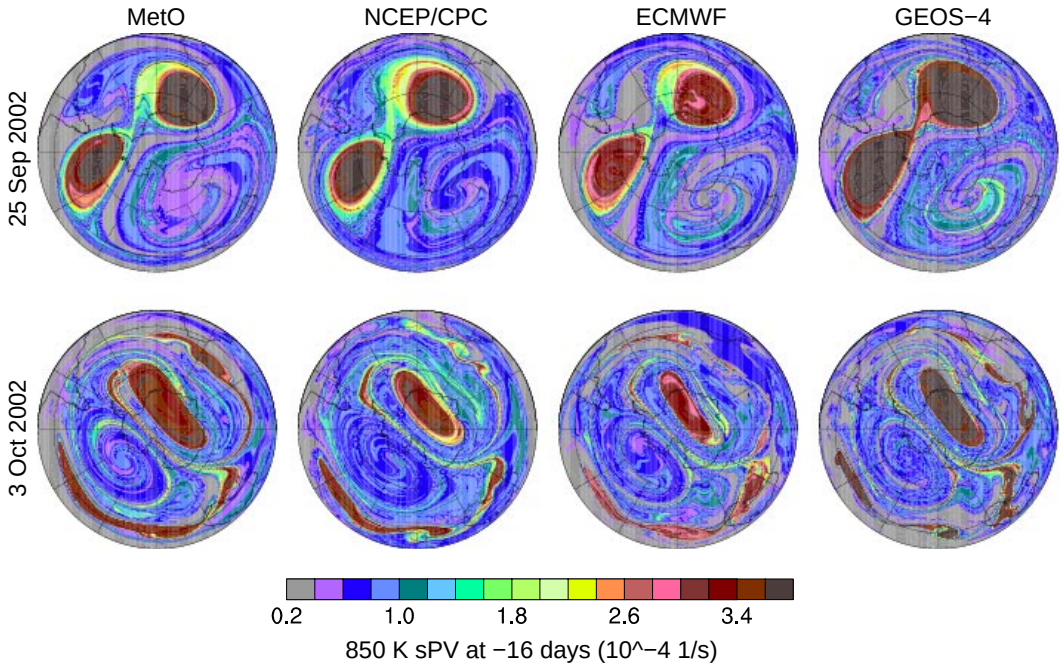

Figure 11. 850-K "PV-tracer" maps on 25 September and 3 October 2002 from high-resolution isentropic trajectory calculations using each of four meteorological analyses. Back trajectories are initialized with sPV 16 days before date shown. Layout is as in Figure 9.

$1\times1.25^\circ$ to $2\times2.5^\circ$ (not shown; and of $2.5\times2.5^\circ$ ECMWF with $1.25\times1.25^\circ$ ECMWF-R results) indicates that only a small part of this arises from using the analysis at higher resolution.

c. Lamination in Trace Gas Profiles

Grooß et al. (2004) and Konopka et al. (2004) show examples where chemical transport model (CTM) calculations driven with ECMWF data reproduced filaments in HALOE (the Halogen Occultation Experiment on UARS) data. We examine filamentation quantitatively here using RT calculations to model small vertical scale laminae in ozone (e.g., Manney et al., 1998, 2000, and references therein). Figure 12 shows two Stratospheric Aerosol and Gas Experiment (SAGE) III ozone profiles with laminar structure in the lower stratosphere observed at different times and longitudes on 23 September – the first with a local maximum (minimum) near 490 (525) K, and the second with a local maximum (minimum) near 480 (540) K. Ten-day reverse trajectory calculations for these profile locations using ECMWF, MetO, NCEP/CPC, and GEOS-4 winds were initialized with "proxy" ozone fields derived from SAGE III, HALOE and Polar Ozone and Aerosol Measurement (POAM) III data (Randall et al., 2004), which are based on reconstructing 3D ozone fields using ozone/PV correlations. The dashed black lines show the proxy ozone used for initialization at the SAGE III observation locations. For the first profile, the proxy field shows no evidence of the lamina pair (suggesting that this feature in ozone does not arise from something that is represented in the PV fields used for proxy reconstruction), while for the second profile, there is a greatly smoothed echo of it (suggesting that there is some indication of this feature in the PV field).

All analyses show a similar maximum/minimum pair for the second profile. There are noticeable differences in the calculations of very small scale structure for this profile, but since these very small scale structures are not represented in the SAGE III profile, we have no way to judge whether one might be more realistic than another. Examination of RT ozone maps (not shown) indicates that this laminae pair arises from the observations crossing the vortex edge between those levels; RT calculations have previously been found to be most successful at the refinement of the representation of gradients along the vortex edge (e.g., Fairlie et al., 1997; Manney et al., 1998), so it is not too surprising that all of the analyses do well in this case (these features are also captured in each analysis for shorter (6-8 day) calculations). In contrast, the laminae pair in the first profile arises from sampling a very narrow filament of lower-ozone (lower-latitude) air drawn into the collar region of

high ozone along the vortex edge, a situation where detailed simulation is much more difficult (e.g., Manney et al., 1998). For this feature, none of the calculations is as successful, but there is large variation in the degree to which the calculations capture any indication of the observed feature. The MetO calculations show little suggestion of a minimum corresponding to that in the SAGE profile, and the NCEP/CPC calculations show only a hint of a minimum near 560 K. The ECMWF analyses and GEOS-4 calculations show a maximum/minimum pair; in all cases it is located a bit higher than in SAGE (near 490/540 K for ECMWF and GEOS-4L, and near 520/560 K for GEOS-4). The vertical resolution of SAGE III ozone ($\sim$0.5 km at these altitudes) is quite adequate for resolving all the larger scale features in the calculations. Preliminary results suggest that average SAGE errors in this altitude range are less than 5%, and that systematic altitude registration errors are negligible (C. E. Randall et al, "Comparisons of SAGE III ozone profiles with satellite and sonde data", in preparation). However, line of sight inhomogeneities can lead to significant random errors in highly structured profiles, which could account for some of the offsets with respect to the RT calculations in Figure 12.

The above diagnostics reveal considerable discrepancies between the analyses in timing, location, and magnitude of regions of enhanced transport and mixing, though representation of the polar vortex transport barrier is reasonably consistent. Our calculations of the development of fine-scale structure show that some of these inter-analysis variations are related to differences in the development and evolution of filaments and the interweaving of narrow tongues of low latitude and vortex air. Development of more filamentary structure and better simulations of laminae in ECMWF and GEOS-4 analyses suggest (as was the case for the PV fields shown in section 4(*b*)) a benefit from higher-resolution assimilation systems, even when their results are used at reduced resolution. The relatively large differences in small-scale structure and mixing imply that significant quantitative differences would be expected in more detailed transport calculations. Such differences could be important to studies like those of Grooß et al. (2004), Konopka et al. (2004), and Marchand et al. (2004) that rely on quantitative modeling of filaments and vortex fragments. Although we have limited temporal and spatial records of high-resolution (vertical and/or horizontal) trace gas data that might help determine which analyses produce more realistic results, more comprehensive studies along the lines of the SAGE lamination example shown above may provide some insight, and future datasets, such as those from EOS (Earth Observing System) Aura, ENVISAT (Environmental Satellite) and the continuing records of SAGE III and POAM III data, can help alleviate this difficulty.

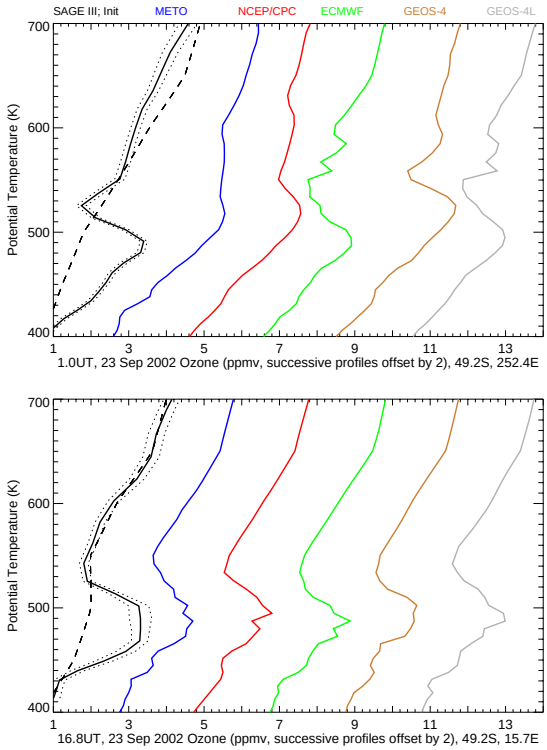

Figure 12. Two SAGE III ozone profiles (thick black curves, with estimated random error as dotted lines), and profiles from high-resolution RT calculations using each of four different meteorological analyses (colors; GEOS-4 is used at its native, "GEOS-4", and reduced, "GEOS-4L" resolution, see text). Dashed black line with SAGE profiles show the profiles at the SAGE III locations from the initialization fields.

6. Polar Processing Diagnostics

Model studies of polar processing (e.g., Sinnhuber et al., 2003; Feng et al., 2004; Grooß et al., 2004; Marchand et al., 2004) depend strongly on temperatures and temperature histories. Figure 13 shows the area where temperatures are low enough for nitric acid trihydrate (NAT) PSC formation as a function of time and pressure for each of the analyses. (The criterion of Hanson and Mauersberger (1988) is used, with HNO_3 and H_2O values from UARS profiles as described by Manney et al. (2003).) As suggested by the minimum temperature plots in Figure 2, the MetO analyses show a slightly larger (0.5 to 1.0% of hemisphere, up to about a 10% difference from the other analyses) cold region than ECMWF, NCEP/CPC, and GEOS-4 between ∼80 and 15 hPa; below this, MetO shows a small high temperature (low area) bias. At and above 10 hPa, NCEP/CPC and GEOS-4 analyses are low with respect to MetO and ECMWF until early August, when biases between these four analyses become negligible.

The REAN2 and ERA-40 reanalyses are included to highlight the problems in their lower stratospheric temperature fields. REAN2 temperatures are biased high with respect to the other analyses by as much as ∼6% of a hemisphere (about a 50% bias) between ∼60 and 10 hPa; this bias is large enough to have a substantial effect on polar processing studies. The oscillatory vertical structure in ERA-40 temperatures results in a much smaller cold region between about 50 and 20 hPa than the other analyses, and the unrealistic temperature structure in August is obvious in the large area of low temperatures near 10 hPa.

Because the SH winter is so cold, with a large fraction of the vortex having temperatures well below both NAT and ice PSC formation thresholds for several months, even the 3–6 K biases seen above between analyses might be expected to result in only small percentage changes in calculations of, e.g., denitrification or ozone loss. As noted by Pawson et al. (1999) for the NH, temperature differences are most likely to have a significant effect on polar processing studies when conditions are marginal for PSC existence, namely in fall or spring in the SH, when the timing of the onset of PSCs or their disappearance may vary, and may affect such studies.

To examine the likelihood and timing of PSC formation in spring and fall, we performed temperature history calculations like those of Manney et al. (2003), with starting dates a few days after the onset of $T \leq T_{NAT}$ in fall and a few days before the disappearance of $T \leq T_{NAT}$ in spring. Calculations are shown at 465 and 585 K, with T_{NAT} taken to be 195 and 193 K, respectively (approximate values from Hanson and Mauersberger, 1988). Parcels were initialized on a dense equal area grid within the region with $T \leq T_{NAT}$, and run twenty days back and twenty days forward using winds from each of the analyses (Manney et al., 2003). Average temperature histories (not shown) indicate similar behavior in fall, but the MetO analyses at 465 K show an earlier onset of temperatures consistently below T_{NAT} by ∼5–6 days. Conversely, the REAN2 analyses at 585 K show a later onset of $T \leq T_{NAT}$ than the other analyses by ∼7–10 days. September average temperature histories show good agreement between all analyses.

As in Manney et al. (2003) we calculate the total number of days that each parcel was at or below T_{NAT} (Figure 14), and the continuous time before and after the initialization date that each of the parcels remained below T_{NAT} (Figure 15). The latter diagnostic is related to PSC duration and denitrification, and can be viewed as an idealized or potential PSC lifetime. The former, giving an indication of the total time when PSCs are present, is related to chlorine activation. Histories from the GEOS-4 reduced resolution fields, ECMWF-R, and REAN are very similar to those for GEOS-4, ECMWF, and REAN2, respectively. At 465 K, there is fair agreement in overall distributions between the analyses in total PSC days (Figure 14), but MetO, and to a lesser degree GEOS-4, analyses for 26 May show stronger peaks at a larger number of days (around 28 and 22 days for MetO and GEOS-4, respectively), and REAN2 analyses show a strong peak near 15 days that is absent in the other analyses. At 585 K, the REAN2 analysis stands out as an outlier, with a strong peak near 25 days for 26 May, as opposed to ∼33-35 days for the other analyses, and a compact distribution contained from 1–7 days for 13 September, as opposed to broad distributions extending to 22–27 days for the other analyses. At 585 K, the NCEP/CPC analyses also stand out on 26 May, compared to the very similar distributions for MetO, ECMWF and GEOS-4. The PSC lifetime distributions (Figure 15) also show significant variation among analyses, especially in the existence of peaks at longer lifetimes (e.g., over 20 days in MetO and REAN2 in May, and in MetO and GEOS-4 in September).

Overall, PSC formation potential and temperature histories in the SH 2002 winter exhibit much better agreement than is typical during the NH winter (Manney et al., 2003); however, there are still differences significant enough to affect the results of polar processing studies. Feng et al. (2004) found lower total ozone values in the 2002 late winter in CTM simulations driven with MetO winds than in those driven with ECMWF winds, consistent with the generally lower MetO temperatures seen here. The REAN/REAN2 results again argue against using these analyses for detailed polar processing studies in the SH.

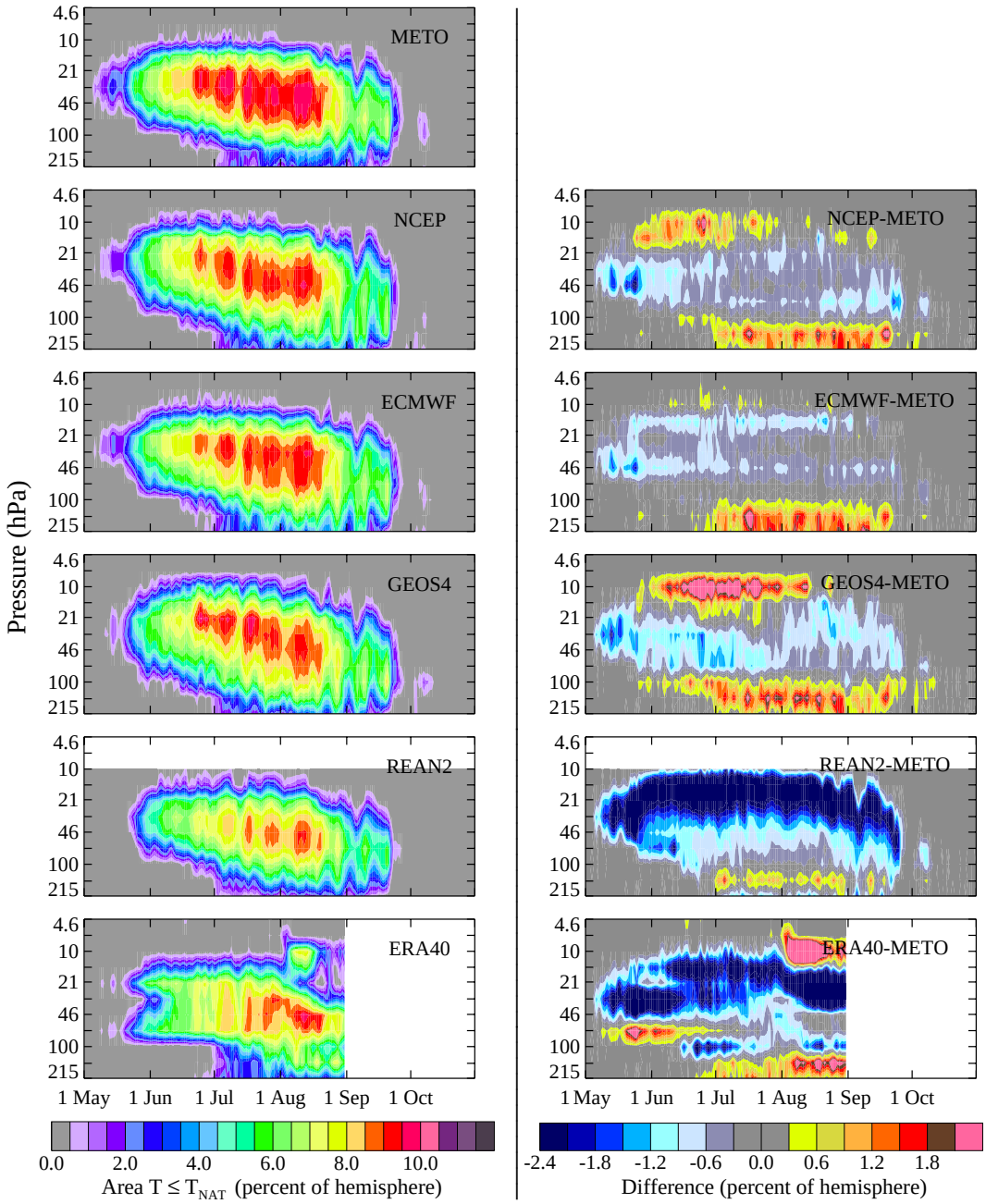

Figure 13. Pressure/time cross-sections of the area with $T \leq T_{NAT}$ (fraction of a hemisphere) for May through October 2002 in the SH (left), from (top to bottom) MetO, NCEP/CPC, ECMWF, GEOS-4, REAN2, and ERA-40 (through August) temperatures, and the difference of each of the areas from those for the MetO analyses (right, blue colors indicate a larger cold region in the MetO analyses).

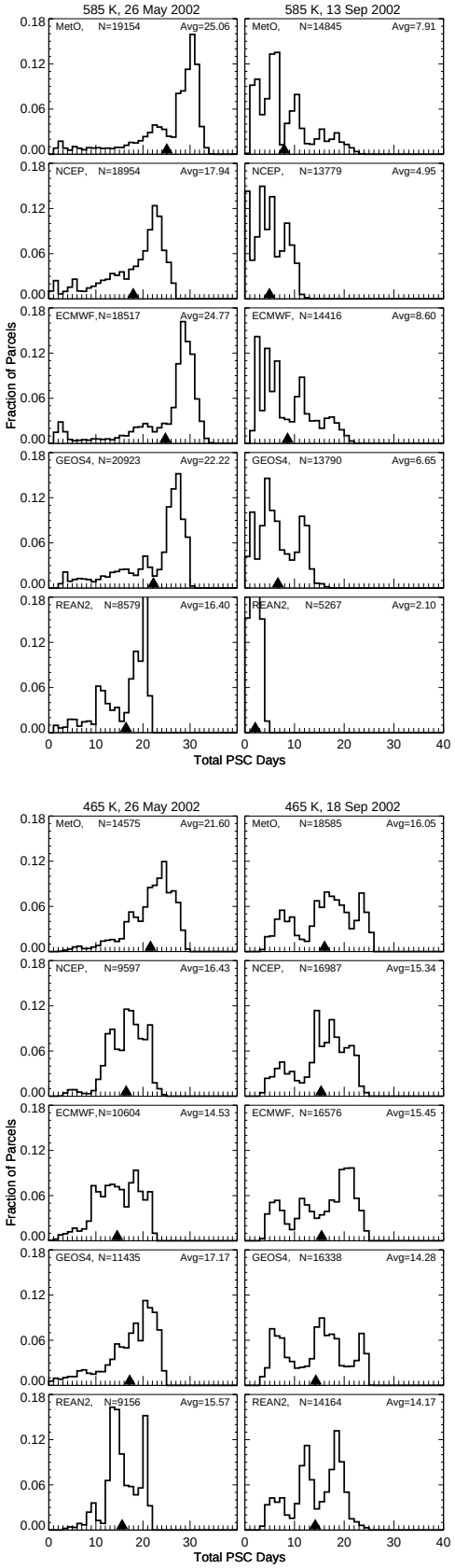

Figure 14. Histograms of the total number of days spent at $T \leq T_{NAT}$ for trajectory runs initialized in the cold region at (top) 585 K and (bottom) 465 K on 26 May 2002 (left) and 13 (18) September 2002 at 585 (465) K (right). Arrows indicate average number of days; number of parcels used and average number of days are given in the labels.

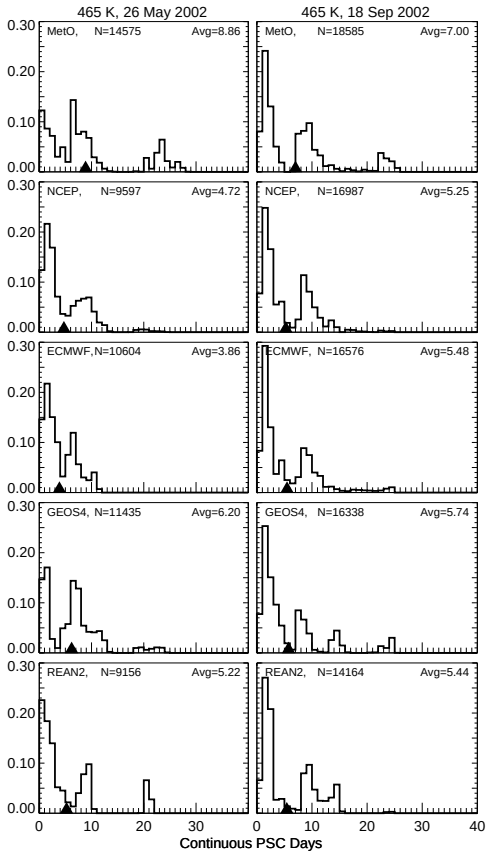

Figure 15. Histograms of the number of days surrounding the initialization time continuously at $T \leq T_{NAT}$ for trajectory runs initialized in the cold region at 465 K on (left) 26 May 2002 and (right) 18 September 2002. Arrows indicate average number of days; number of parcels used and average number of days are given in the labels.

7. Summary and Conclusions

Most studies of the unique SH 2002 winter rely on gridded meteorological data from one of several commonly used analysis systems, and the dataset used can influence the results. We have compared diagnostics related to temperature evolution and lower stratospheric chemistry, quasi-isentropic transport and mixing, and large-scale dynamical evolution for four operational products (MetO, ECMWF, NCEP/CPC and GEOS-4) as well as the ERA-40 and REAN/REAN2 reanalyses to assess to what degree the conclusions of scientific studies may be affected by the choice of meteorological analysis.

Examination of the evolution of temperatures, winds, waves, and synoptic fields provides a very consistent picture of the large-scale dynamics of the SH 2002 winter between the analyses, indicating high confidence in many observational studies, regardless of which meteorological dataset is used. However, REAN/REAN2 analyses frequently overestimate minima and underestimate maxima in lower stratospheric temperature. Similar, but less severe, shortcomings are seen in the NCEP/CPC data. REAN/REAN2 lower stratospheric temperatures are significantly higher than those in other analyses, and the differences increase with height. ERA-40 Antarctic temperatures show persistent, unrealistic vertically oscillatory structure in the SH 2002 winter (Simmons et al., 2004) and additional degradation in August 2002. REAN/REAN2 winds and EP fluxes also show increasing differences (weaker winds and EP flux divergences) in the top few levels where they are available (between about 30 and 10 hPa), which could influence the results of detailed studies. Quantitative agreement between upper-stratospheric wind fields in all the analyses is lacking, and larger variations are seen in temperature structure near the stratopause. Low-latitude upper-stratospheric winds show substantial differences in the representation of the SAO, with ECMWF, ECMWF-R, ERA-40, and GEOS-4 giving qualitatively similar pictures, but MetO showing SAO westerlies only at considerably higher altitudes. Larger differences are expected in the upper stratosphere, where the assimilation systems are only weakly constrained by data. There are also substantial differences in vortex strength, structure and evolution in the upper stratosphere, with the NCEP/CPC objective analyses giving a cruder representation of these features. Differences such as these may have only a small effect on observational studies, but are expected to be significant in modeling and in more detailed studies of large-scale dynamics, including those of synoptic morphology and vortex evolution.

Diagnostics relevant to transport and CTM modeling show greater variations. The polar vortex transport barrier is similar in all of the analyses; however, there is little consensus on the amount, patterns and timing of mixing in midlatitudes, or on the extent of mixing into the polar regions during the major warming. Some variations in mixing between analyses are related to differences in development, location and evolution of filamentary structure. REAN2 shows much less mixing in the lower stratosphere than the other analyses. In the examples presented here, ECMWF and GEOS-4 analyses do best at representing filamentation and lamination, suggesting that higher resolution assimilation systems benefit such studies, even when reduced-resolution fields from those systems are used. Temperature history calculations relevant to polar process modeling show the REAN/REAN2 analyses to be an outlier, predicting significantly shorter PSC lifetimes and less potential for chlorine activation than the other analyses. While MetO temperature history results show slightly longer PSC lifetimes and more activation potential, these differences are much smaller than those between REAN/REAN2 and the other analyses.

The comparisons presented here highlight limitations that make some of the datasets inappropriate for certain studies. The REAN/REAN2 analyses were primarily designed for studying the troposphere (Kalnay et al., 1996); they have badly biased temperatures in the lower stratosphere and do not adequately represent dynamical events above $\sim$50 hPa. The NCEP/CPC objective analyses have been very valuable in the past, facilitating groundbreaking studies of middle atmosphere dynamics. However, compared to the assimilated datasets now available, they suffer from the assumptions that must be made in deriving dynamical fields. Assimilated fields, such as those from ECMWF, MetO and GEOS-4, represent dynamical features such as filamentation. Even though there are significant quantitative differences between the analyses, they provide an adequate physical representation of certain mixing processes. It will be a major challenge for future analyses to represent these consistently in a synoptic (rather than a statistical) manner.

The most important studies in which to consider the effects of choosing one of these analyses are detailed chemistry and transport modeling studies (including polar processing), as well as more detailed studies of synoptic evolution and fine-scale structure in dynamical fields (especially in the upper stratosphere). Some research efforts are already assessing these effects by repeating calculations driving models with more than one of these analyses (e.g., Feng et al., 2004; Manney et al., 2004). In the areas where there is least consensus among the analyses – detailed 3D synoptic evolution, transport, mixing, and development of fine-scale structure – we currently have few data available to help to determine which results are accurate. While some progress can be made with more extensive studies of lamina-

tion and filamentation captured in aircraft and/or sparse profile data, such transient or localized observations rely heavily on luck in capturing these small-scale features, and do not help in assessing large-scale transport or 3D vortex evolution. However, in the very near future we will see a dramatic increase in large-scale, global, and in some cases relatively high-resolution, long-lived trace gas fields and temperature data extending through the mesosphere. Some such fields are beginning to be available from MIPAS (Michelson Interferometer for Passive Atmospheric Sounding) and SCIAMACHY (Scanning Imaging Absorption Spectrometer for Atmospheric Chartography) on ENVISAT, and additional fields will be available from the MLS (Microwave Limb Sounder) and HIRDLS (High Resolution Dynamics Limb Sounder) instruments on EOS Aura (to be launched in June 2004). As such fields become more readily available, we will see a great improvement in our ability to quantitatively assess the accuracy of global meteorological datasets.

Acknowledgments. Thanks to the UK Met Office and the British Atmospheric Data Centre for MetO data, the GSFC ACD Science Data System (Eric Nash and Paul Newman) for NCEP/CPC Data, the German Weather Service (Deutscher Wetterdienst, DWD) for ECMWF, ERA-40 and radiosonde data, ECMWF for ECMWF-R data and NASA's GMAO for GEOS-4 data; NCEP Reanalysis and Reanalysis-2 data were provided by the NOAA-CIRES Climate Diagnostics Center, Boulder, Colorado, USA, from their web site at http://www.cdc.noaa.gov/. SAGE III data were obtained from the NASA Langley Research Center Atmospheric Sciences Data Center. We thank the JPL MLS team for technical assistance, data management and computer support, Paul Newman for original routines used to calculate PV, Kathrin Schöllhammer and Markus Kunze for obtaining and processing ECMWF ω data, Wesley Ebisuzaki for information on REAN/REAN2 data, and Sara Amina Sena for graphics, analysis and data management assistance. The supercomputer used in this investigation was provided by the Jet Propulsion Laboratory, California Institute of Technology (JPL/CalTech) supercomputing project, which is funded by the NASA Offices of Earth Sciences, Aeronautics and Space Science. Work at JPL/CalTech was done under contract with the National Aeronautics and Space Administration.

References

Allen, D. R., R. M. Bevilacqua, G. E. Nedoluha, C. E. Randall, and G. L. Manney, 2003: Unusual stratospheric transport and mixing during the 2002 Antarctic winter. *Geophys. Res. Lett.*, **30**, 1599, doi:10.1029/2003GL017117.

Allen, D. R. and N. Nakamura, 2001: A seasonal climatology of effective diffusivity in the stratosphere. *J. Geophys. Res.*, **106**, 7917–7935.

—, 2003: Tracer equivalent latitude: A diagnostic tool for isentropic transport studies. *J. Atmos. Sci.*, **60**, 287–304.

Cohn, S. E., A. da Silva, J. Guo, M. Siekenwicz, and D. Lamich, 1998: Assessing the effects of data selection with the DAO physical-space statistical analysis system. *Mon. Weather Rev.*, **126**, 2913–2926.

Douglass, A. R., M. R. Schoeberl, R. B. Rood, and S. Pawson, 2003: Evaluation of transport in the lower tropical stratosphere in a global chemistry and transport model. *J. Geophys. Res.*, **108**, 4259, doi:10.1029/2002JD002696.

Dunkerton, T. J. and D. P. Delisi, 1986: Evolution of potential vorticity in the winter stratosphere of January-February 1979. *J. Geophys. Res.*, **91**, 1199–1208.

Fairlie, T. D. A., M. Fisher, and A. O'Neill, 1990: The development of narrow baroclinic zones and other small-scale structure in the stratosphere during simulated major warmings. *Q. J. R. Meteorol. Soc.*, **116**, 287–315.

Fairlie, T. D. A., R. B. Pierce, W. L. Grose, G. Lingenfelser, M. Loewenstein, and J. R. Podolske, 1997: Lagrangian forecasting during ASHOE/MAESA: Analysis of predictive skill for analyzed and reverse-domain-filled potential vorticity. *J. Geophys. Res.*, **102**, 13,169–13,182.

Feng, W., M. P. Chipperfield, H. K. Roscoe, J. J. Remedios, A. M. Waterfall, G. P. Stiller, N. Glatthor, M. Höpfner, and D.-Y. Wang, 2004: Three-dimensional model study of the Antarctic ozone hole in 2002 and comparison with 2000, *J. Atmos. Sci., accepted*.

Gray, L. J., W. Norton, C. Pascoe, and A. Charlton, 2004: A possible influence of equatorial winds on the September 2002 southern hemisphere sudden warming event, *J. Atmos. Sci., accepted*.

Grooß, J.-U., P. Konopka, and R. Müller, 2004: Ozone chemistry during the 2002 Antarctic vortex split, *J. Atmos. Sci., submitted*.

Hanson, D. and K. Mauersberger, 1988: Laboratory studies of the nitric acid trihydrate: Implications for the south polar stratosphere. *Geophys. Res. Lett.*, **15**, 855–858.

Harnik, N., R. K. Scott, and J. Perlwitz, 2004: Wave reflection and focusing prior to the major stratospheric warming of September 2002, *J. Atmos. Sci., submitted*.

Haynes, P. and E. Shuckburgh, 2000a: Effective diffusivity as a diagnostic of atmospheric transport 1. stratosphere. *J. Geophys. Res.*, **105**, 22,777–22,794.

—, 2000b: Effective diffusivity as a diagnostic of atmospheric transport 2. troposphere and lower stratosphere. *J. Geophys. Res.*, **105**, 22,795–22,810.

Hio, Y. and S. Yoden, 2004: Interannual variations of the seasonal march in the southern hemisphere stratosphere for 1979–2002 and characterization of the unprecedented year 2002, *J. Atmos. Sci., accepted*.

Hoppel, K. W., R. Bevilacqua, G. Nedoluha, C. Deniel, F. Lefevre, J. Lumpe, M. Fromm, C. Randall, J. Rosenfield, and M. Rex, 2003: POAM III observations of the anomalous 2002 Antarctic ozone hole. *Geophys. Res. Lett.*, **30**, 1394, doi:10.1029/2003GL016899.

Kalnay, E. et al., 1996: The NCAR/NCEP 40-year reanalysis project. *Bull. Am. Meteorol. Soc.*, **77**, 437–471.

Kanamitsu, M., W. Ebisuzaki, J. Woollen, S.-K. Yang, J. J. Hnilo, M. Fiorino, and G. L. Potter, 2002: NCEP-DOE AMIP-II reanalysis (R-2). *Bull. Am. Meteorol. Soc.*, **83**, 1631–1643.

Konopka, P., J.-U. Grooß, K. W. Hoppel, H.-M. Steinhorst, and R. Müller, 2004: Mixing and chemical ozone loss during and after the Antarctic polar vortex major warming in September 2002, *J. Atmos. Sci., submitted*.

Krüger, K., B. Naujokat, and K. Labitzke, 2004: The unusual midwinter warming in the southern hemisphere stratosphere 2002: A comparison to northern hemisphere phenomena, *J. Atmos. Sci., accepted*.

Li, S., S. Pawson, B. A. Boville, and S.-J. Lin, 2004: Sensitivity of middle atmospheric analysis to the representation of gravity wave drag, *J. Atmos. Sci., submitted*.

Lin, S.-J., 2004: A vertically Lagrangian finite-volume dynamical core for global models, *Mon. Wea. Rev., in press*.

Lorenc, A. C. et al., 2000: The Met. Office global three-dimensional variational data assimilation scheme. *Q. J. R. Meteorol. Soc.*, **126**, 2991–3012.

Manney, G. L., J. C. Bird, D. P. Donovan, T. J. Duck, J. A. Whiteway, S. R. Pal, and A. I. Carswell, 1998: Modeling ozone laminae in ground-based Arctic wintertime observations using trajectory calculations and satellite data. *J. Geophys. Res.*, **103**, 5797–5814.

Manney, G. L., J. D. Farrara, and C. R. Mechoso, 1994a: Simulations of the February 1979 stratospheric sudden warming: Model comparisons and three-dimensional evolution. *Mon. Weather Rev.*, **122**, 1115–1140.

Manney, G. L., H. A. Michelsen, F. W. Irion, M. R. Gunson, G. C. Toon, and A. E. Roche, 2000: Lamination and polar vortex development in fall from ATMOS long-lived trace gases observed during November 1994. *J. Geophys. Res.*, **105**, 29,023–29,038.

Manney, G. L., J. L. Sabutis, D. R. Allen, W. A. Lahoz, A. A. Scaife, C. E. Randall, S. Pawson, B. Naujokat, and R. Swinbank, 2004: Simulations of dynamics and transport during the September 2002 Antarctic major warming, *J. Atmos. Sci., accepted*.

Manney, G. L., J. L. Sabutis, S. Pawson, M. L. Santee, B. Naujokat, R. Swinbank, M. E. Gelman, and W. Ebisuzaki, 2003: Lower stratospheric temperature differences between meteorological analyses in two cold Arctic winters and their impact on polar processing studies. *J. Geophys. Res.*, **108**, 8328, doi:10.1029/2001JD001149.

Manney, G. L., R. Swinbank, S. T. Massie, M. E. Gelman, A. J. Miller, R. Nagatani, A. O'Neill, and R. W. Zurek, 1996: Comparison of U. K. Meteorological Office and U. S. National Meteorological Center stratospheric analyses during northern and southern winter. *J. Geophys. Res.*, **101**, 10,311–10,334.

Manney, G. L., R. W. Zurek, A. O'Neill, and R. Swinbank, 1994b: On the motion of air through the stratospheric polar vortex. *J. Atmos. Sci.*, **51**, 2973–2994.

Marchand, M., S. Bekki, A. Pazmino, F. Lefèvre, S. Godin-Beekmann, and A. Hauchecorne, 2004: Model simulations of the impact of the 2002 Antarctic ozone hole on midlatitudes, *J. Atmos. Sci., accepted*.

Nedoluha, G. E., R. M. Bevilacqua, M. D. Fromm, K. W. Hoppel, and D. R. Allen, 2003: POAM measurements of PSCs and water vapor in the 2002 Antarctic vortex. *Geophys. Res. Lett.*, **30**, 1796, doi:10.1029/2003GL017577.

Newman, P. A., L. R. Lait, M. R. Schoeberl, R. M. Nagatani, and A. J. Krueger, 1989: Meteorological atlas of the Northern Hemisphere lower stratosphere for January and February 1989 during the Airborne Arctic Stratospheric Expedition. Tech. Rep. 4145, NASA.

Newman, P. A. and E. R. Nash, 2004: The unusual southern hemisphere stratosphere winter of 2002, *J. Atmos. Sci., accepted*.

Pawson, S., K. Krüger, R. Swinbank, M. Bailey, and A. O'Neill, 1999: Intercomparison of two stratospheric analyses: Temperatures relevant to polar stratospheric cloud formation. *J. Geophys. Res.*, **104**, 2041–2050.

Randall, C. E., G. L. Manney, D. R. Allen, R. M. Bevilacqua, C. Trepte, W. A. Lahoz, and A. O'Neill, 2004: Reconstruction and simulation of stratospheric ozone distributions during the 2002 austral winter, *J. Atmos. Sci., accepted*.

Randel, W. J., 1987: The evaluation of winds from geopotential height data in the stratosphere. *J. Atmos. Sci.*, **44**, 3097–3120.

Randel, W. J. et al., 2004: The SPARC intercomparison of middle atmosphere climatologies. *J. Clim.*, **17**, 986–1003.

Rogers, H. L., W. A. Norton, A. Lambert, and R. G. Grainger, 1999: Isentropic, diabatic, and sedimentary transport of Mount Pinatubo aerosol. *J. Geophys. Res.*, **104**, 4051–4063.

Sabutis, J. L., 1997: The short-term transport of zonal mean ozone using a residual mean circulation calculated from observations. *J. Atmos. Sci.*, **54**, 1094–1106.

Scaife, A. A., R. Swinbank, D. R. Jackson, N. Butchart, H. Thornton, M. Keil, and L. Henderson, 2004: Stratospheric vacillations and the major warming over Antarctica in 2002, *J. Atmos. Sci., submitted*.

Schoeberl, M. R., A. R. Douglass, Z. Zhu, and S. Pawson, 2003: A comparison of the lower stratospheric age spectra derived from a general circulation model and two data assimilation systems. *J. Geophys. Res.*, **108**, 4113, doi:10.1029/2002JD002652.

Siegmund, P., H. Eskes, and P. van Velthoven, 2004: Antarctic ozone transport and depletion in Austral spring 2002, *J. Atmos. Sci., accepted*.

Simmons, A. J., M. Hortal, G. Kelly, A. McNally, A. Untch, and S. Uppala, 2004: ECMWF analyses and forecasts of stratospheric winter polar vortex break-up: September 2002 in the southern hemisphere and related events, *J. Atmos. Sci., accepted*.

Sinnhuber, B.-M., M. Weber, A. Amankwah, and J. P. Burrows, 2003: Total ozone during the unusual Antarctic winter of 2002. *Geophys. Res. Lett.*, 1580, doi:10.1029/2002GL016798.

Swinbank, R., N. B. Ingleby, P. M. Boorman, and R. J. Renshaw, 2002: A 3D variational data assimilation system for the stratosphere and troposphere. Tech. Rep. 71, Met Office Numerical Weather Prediction Forecasting Research Scientific Paper.

Tan, W. W., M. A. Geller, S. Pawson, and A. da Silva, 2004: A case study of excessive subtropical transport in the stratosphere of a data assimilation system, *J. Geophys. Res., in press*.

This preprint was prepared with AGU's LaTeX macros v5.01. File sh2002comp˙pp formatted April 29, 2004.